Prepared for submission to JINST

Doping liquid argon with xenon in ProtoDUNE Single-Phase

D.L. Adams, M.C.Q. Bazetto, L. Bomben, S. Bordoni, F. Boran, C. Brizzolari, G. Brunetti, C. Cattadori, F. Cavanna, G. De Souza, F. Dolek, Z. Djurcic, A. Falcone, N. Gallice, A. Himmel, U. Kose, E. Lutsenko, A.A. Machado, F. Pietropaolo, M. Prest, A. Rafique, B. Ramson, F. Resnati, P. Sala, E. Segreto, K. Spurgeon, H. Vieira de Souza, D. Totani, S. Tufanli, E. Vallazza, D. Warner, D. Whittington, R.J. Wilson, A. Zani

Abstract: Doping of liquid argon TPCs (LArTPC) with a small concentration of xenon is a well-known technique for light-shifting and eases the detection of the liquid argon scintillation light. In this paper, we present the results of the first doping test ever performed in a kton scale LArTPC. From February to May 2020, we carried out this special run in the DUNE Single Phase ProtoDUNE prototype (ProtoDUNE-SP) at CERN, featuring a mass of 770 tons of liquid argon (fiducial: 400 tons). The goals of the run were to measure the light and charge response of the detector to xenon up to a concentration of 20 ppm, reduce the non-uniformities in light collection caused by the location of the DUNE photosensors in the anode only, and compensate for light losses due to air contamination. Light collection was analysed as a function of the xenon concentration, by using the ProtoDUNE Photon Detection System (PDS) and a dedicated setup installed before the run. In this paper we review the physics of xenon doping and the injection method deployed in ProtoDUNE-SP. Then, we discuss the obtained results, which demonstrate a successful procedure. We are able to disentangle argon and xenon light intensity and measure their dependence on the dopant concentration; we perform studies of the collection efficiency as a function of the distance between tracks and light detectors, obtaining enhanced uniformity of response. Incidentally, we show that xenon doping can help recovering from light losses due to contamination of the liquid argon.

Keywords: Noble liquid detectors (scintillation, ionization, double-phase); Neutrino detectors

Contents

1 Introduction

Liquid Argon Time Projection Chambers (LArTPC, [1]) are prominent in contemporary physics for the study of neutrino oscillations and the search for rare events, including Dark Matter [2–5]. This technology has been developed for more than 40 years and reached a level of sophistication scalable up to multi-kilotonnes detectors. DUNE, in particular, is designing and constructing four underground modules with a total mass of 17 kt each, which will be located at the Sanford Underground Research Facility (SURF) in South Dakota, USA. Its main goal is the precise determination of neutrino oscillation parameters, which will be achieved mainly with beam neutrinos; other than that, atmospheric, supernovae and solar neutrino detection, as well as proton decay and Beyond the Standard Model (BSM) physics searches, are planned [6, 7]. A LArTPC exploits the deposited ionization charge in argon, drifted towards the anode plane, to perform spatial and calorimetric reconstruction of events. Furthermore, liquid argon (LAr) is a high-performance scintillator. It emits light in the Vacuum UltraViolet (VUV) region with a spectrum centered at λ = 128 nm and a yield of about 4×10^4 (2.4×10^4) photons/MeV at 0 V/cm (500 V/cm) electric field. The scintillation light is produced by de-excitation of the singlet ($\tau_s \simeq 6$ ns) and triplet ($\tau_l \simeq 1.3\ \mu$s) states of the unstable excited dimer Ar_2^*; their ratio depends on the energy loss mechanism and can be used for particle identification by the analysis of the pulse shape.

Detecting VUV light in liquid argon is challenging but the physics advantages are remarkable, especially in DUNE. The scintillation light provides the t_0 to the TPC and the third coordinate of the interaction. It then improves by one order of magnitude (1 cm $\rightarrow$ 1 mm) the localization of the interaction vertex, with respect to the t_0 provided by the proton kicker of the neutrino beam (LBNF for DUNE). Furthermore, light collection is the main tool to trigger events that are not produced by the beam and plays a special role in triggering and recording supernovae neutrino bursts. The light is also anti-correlated with the ionization loss of the particle and can be exploited for combined charge-light calorimetry. A high light collection efficiency can outperform the TPC energy resolution, especially for low energy events [8].

The DUNE Photon Detection System (PDS) can be enhanced by doping LAr with xenon at the level of few tens of ppm[1]. DUNE is exploring this opportunity because the longer Rayleigh scattering length of the shifted light in LAr should increase the light collection far from the photon detectors. Furthermore, the xenon emission can be collected with higher efficiency due to its longer wavelength. Previous literature studies ([9–13]) have demonstrated the doping procedure on small scale detectors, and sometimes in gas phase. In order to test the feasibility of such operation in DUNE, it is necessary to perform it at an intermediate scale: therefore, a dedicated xenon doping run was performed with the 770 t Single Phase DUNE ProtoType at CERN (ProtoDUNE Single-Phase, SP) [14, 15] in 2020, which represents a new milestone in the development of very-large-volume LArTPCs.

The ProtoDUNE-SP PDS was enhanced with the addition of two prototypes of X-ARAPUCA photon detectors, i.e. the technology that was selected for deployment in the first module of the DUNE Far Detector (called FD1).

[1]In this paper, unless otherwise specified, the fractional amounts ppm, ppb, ppt (parts per million/billion/trillion) are to be intended as expressing fractions of *mass*.

In this paper, we describe the preparation and the results of the xenon doping run of ProtoDUNE-SP, obtained both with the X-ARAPUCA and the standard PDS. Physics of xenon-doped liquid argon is introduced in Section 2; ProtoDUNE-SP and its Photon Detection System is described in Section 3, after which the actual xenon doping procedure is detailed 4. The analysis of the data recorded by the X-ARAPUCA is presented in Section 5; the studies performed with the main PDS are instead shown in Section 6. Finally, we used the TPC of ProtoDUNE-SP to evaluate the effect of the xenon presence on the charge collection, as discussed in Section 7.

2 Xenon doping of liquid argon

In order to enhance the response of the DUNE PDS, the DUNE Collaboration has been considering the possibility of doping liquid argon with xenon, mainly due to the more favourable physical properties of its scintillation light: these have been investigated in literature on a number of smaller detectors over the years (see for instance [9–13]).

2.1 Xenon basic properties

Xenon is a noble cryogenic liquid as argon and it is exploited in various direct Dark Matter search experiments [16, 17]. Indeed, it has more favorable properties with respect to argon (e.g. higher density, atomic number and electron mobility), that make it appealing as primary target/detecting medium in dual-phase TPCs for Dark Matter searches. On the other hand, due to its low availability and high production cost, its use in particle physics is quite limited.

Xenon liquefies at 165 K and freezes at 161 K. It is a high-yield scintillator as argon: the average energy needed to produce a scintillation photon in xenon is slightly lower than that of argon, for both low- and high-ionization density particles [18]: this results in a slightly higher photon yield ($> 4.2 \times 10^4$ photons/MeV without electric field). Xenon scintillation light is emitted at 178 nm, still in the Ultra-Violet (UV) but in a region where commercial photo-detectors are reasonably sensitive (see below). It features two components, as argon, both much faster than the argon triplet light (4 and 22 ns).

2.2 Doping liquid argon with xenon and its advantages

Converting liquid argon scintillation light to a larger wavelength has significant advantages in a LArTPC, especially if the shift can be performed uniformly within the drift volume, instead than on the photo-sensitive devices (as it happens for standard wavelenght-shifting, WLS, coatings). At the xenon wavelength (178 nm), light detectors with high enough sensitivity are already commercially available (both PMTs and SiPMs). For example, the PDE of last-generation SiPMs at that wavelength exceeds 25% (citation). This would ensure quite efficient collection of the xenon light, allowing the removal of further wavelength-shifting elements, like Tetra-Phenyl Butadiene (TPB).

Furthermore, the faster de-excitation decay time constants of xenon (4 and 22 ns), with respect to argon, contributes to faster pulse profiles. Even considering the convolution of the various processes involved in argon-xenon excitation transfer, one can obtain signals with an overall decay constant of few hundreds ns. Finally, the Rayleigh scattering length in liquid argon at 178 nm is significantly larger than that at 128 nm. This is largely due to the fact that argon refraction index n is rapidly decreasing in the Ultra-Violet region of the spectrum, as a function of increasing wavelength [19]. In the framework of an experiment like DUNE, with very large drift distances involved, this should help obtaining a more uniform response, in terms of photons reaching the light detectors, as a function of the distance from the detectors themselves. In turn, this will allow enhancing the detection efficiency for low energy events (not beam-related) far from the light detectors.

The mentioned properties of xenon make it the more appealing for use as a dopant in the DUNE LAr-TPCs, the larger the drift distance. The present plan is to employ it in a LArTPC geometry different from the one of ProtoDUNE-SP, i.e., a vertical drift TPC with a 6 m drift that will be installed ad DUNE Far Detector 2 (FD2, [20]).

2.3 Principles of xenon doping in LAr

As xenon solidifies at 161 K, its dilution in argon must be performed with extreme care, in order to avoid its freezing. Usually, its concentration in previous experiments ranges from few ppm to few ‰, with light shifting effects setting on already at the few ppm level (citation). According to present models (citation), xenon atoms in suspension in liquid argon interfere with the light production process that involves the argon excited dimers Ar_2^*. Dimers might form in two states, a singlet one $^1\Sigma_u^+$ characterized by a fast decay constant (6 ns, thus dubbed in the following "fast component"), and a triplet state $^3\Sigma_u^+$ with a much larger decay time (∼1300 ns, "slow component").

As shown in Figure 1, in the presence of xenon, a non-radiative collision of a first xenon atom with the dimer leads to the formation of a new hybrid dimer $ArXe^*$, whereas the interaction of a second Xe atom yields a full transfer of energy to a Xe_2^* dimer, which is at this point the entity decaying with emission of light, at 178 nm. The time constants of these two transition processes are identified in Figure 1 as τ_{AX} and τ_{XX}, and they depend directly on the xenon concentration. At relatively low concentrations, below 1 ppm, the double interaction has a low enough probability to let a certain number of hybrid dimers $ArXe^*$ survive long enough to de-excite, producing an intermediate light component around 150 nm [21]. This hybrid component is expected to disappear as the concentration increases to few ppm.

The effect of xenon doping on the collected scintillation light is mainly that the number of photons emitted from the long-lived triplet state of the Ar_2^* dimer ($^3\Sigma_u^+$) drops significantly, as the dimer is destroyed by the collision with xenon atoms. Overall, the total light emitted is characterised by smaller decay-time constants, given by the presence of xenon. The characteristic time profile of the liquid argon scintillation pulse is modified by the presence of xenon, in a way that is proportional to its concentration. This effect will be illustrated in more detail when discussing the data collected in ProtoDUNE SP in Sections 5 and 6.

According to literature(e.g. [22] and references therein), the presence of few ppm of xenon in LAr is sufficient to shift a significant portion of 128 nm LAr photons to xenon scintillation wavelength. In a detector like ProtoDUNE-SP, this translates into injecting few kg of xenon in the LAr bulk: for this reason, it was deemed feasible and important to use the detector as a test-bed for the study of the effects of xenon-doping at large scale. It is worth noting that doping such a large detector has never been attempted before and the long-term behaviour of xenon in LAr was never investigated at this scale.

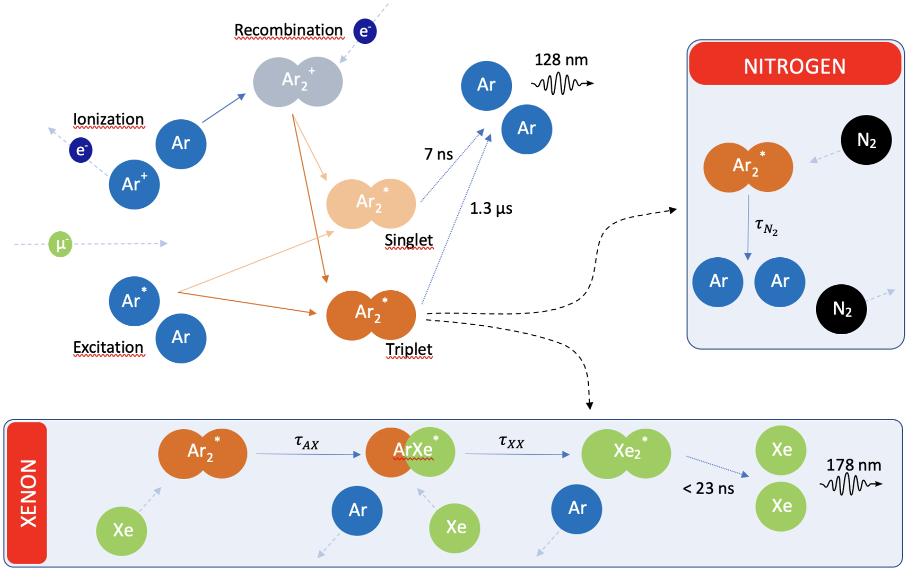

Figure 1: Schematic representation of the production process of scintillation light in pure liquid argon, with concurrent effects nitrogen quenching and xenon doping. The time constants of the non-radiative energy-transfer processes τ_{AX} and τ_{XX} depend on the xenon concentration in LAr.

2.4 Effect of nitrogen contamination in LAr

As discussed in [23], the presence of nitrogen in liquid argon affects scintillation light emission. This is a well-known process called quenching, where the non-radiative collisional reaction $Ar_2^* + N_2 \longrightarrow 2Ar + N_2$ destroys the argon triplet excimers before de-excitation.

Given the characteristics of the xenon interaction with the long-lived triplet state argon dimers, this process can be competitive with the mentioned light quenching [22]. Indeed, it appears to have a larger interaction cross-section, with respect to quenching. For this reason, while introducing its own advantages to scintillation light collection, xenon doping can also help in negating the effects of pollutants in liquid argon, recovering light that would otherwise be lost. This was the case for ProtoDUNE-SP, which experienced an unexpected accident with an argon recirculation pump, introducing a non-negligible amount of nitrogen in the liquid bulk (see Section 4.1).

In the ternary mixture Ar-N_2-Xe, the concurrent processes below are expected, schematised in Figure 1:

- Ar_2^* dimers would normally decay to 2 Ar atoms by emitting light at 128 nm, with the usual two very different decay times already mentioned;
- If a quencher like N_2 is present in the liquid, non-radiative interactions with the quencher can cause dimer destruction, without light emission [23]. The most affected species is the Ar_2^* triplet state $^3\Sigma_u^+$, due to its very large life-time;
- if xenon is also present in LAr, its non-radiative interactions with the long-lived triplet states of Ar_2^* become concurrent with those due to nitrogen, and can lead to the formation of mixed excited state $ArXe^*$;

- according to the concentration of xenon (up to around 1 ppm), a fraction of $ArXe^*$ molecules will de-excite, emitting a characteristic 150 nm radiation [21]. The rest (all of them at higher concentrations) will interact again with single xenon atoms, producing Xe_2^* dimers that will then decay emitting 178 nm photons,
- nitrogen can in principle affect all the reactions mentioned above, but the time scales of all those interactions involving xenon are short enough to be less affected by nitrogen itself.

A more detailed discussion about the modelization of the ternary mixture and its characterization in large volume LArTPCs is deferred to a later publication

$$Ar_2^* + N_2 \rightarrow 2\,Ar + N_2 \tag{2.1}$$

$$Ar_2^* + Xe \rightarrow ArXe^* + Ar \tag{2.2}$$

$$ArXe^* + Xe \rightarrow Xe_2^* + Ar \tag{2.3}$$

$$Xe_2^* \rightarrow Xe + Xe + \gamma\,(178\,nm) \tag{2.4}$$

3 The ProtoDUNE Single-Phase detector

The ProtoDUNE single-phase LArTPC (ProtoDUNE-SP) is a full scale prototype for the first module of the DUNE FD1 [7]. With a total LAr mass of 0.77 kt, it is the largest single-phase LArTPC detector built to date. It is located in the dedicated extension of the EHN1 hall in CERN North Area, where a tertiary portion was added to the existing H4 beam-line, to provide very low-energy charged-particle beams, as part of the CERN Neutrino Platform program. Construction, installation and commissioning of ProtoDUNE-SP detector was completed in July 2018, and is reported in [14]. Immediately after LAr filling and detector activation, beam data were collected in the 0.3-7 GeV range from September to November 2018 [15]. After the beam run, it operated until July 2020 collecting data with cosmics, to validate the design solutions for the future DUNE far detector modules, demonstrate operational stability, and eventually to perform R&D on different aspects of LArTPC technology. Doping LAr with xenon to enhance the light collection of the photon detectors, as presented in this paper, was part of such an R&D effort: an extended test was performed during the last six months before the end of operations of ProtoDUNE-SP.

ProtoDUNE-SP TPC has 411 tons of active LAr volume with dimensions of 6.0 m × 6.9 m × 7.2 m. As shown in Fig. 2, the active volume is split in two by a central cathode plane, defining two identical volumes, with 3.6 m of drift length. The cathode is biased to -180 kV, providing a uniform 500 V/cm electric field in the drift region. On both sides of the cathode, at a distance of 3.6 m, the anode planes assemblies (APAs) are installed. Each APA is made up of four layers of wire planes (three active + a grid layer) for charge readout. Each drift volume is read-out by three APAs. The two volumes are called Left chamber and Right chamber, according to their position along the direction of the incoming charged-particle beam.

3.1 Photon Detection System

Photons produced by LAr scintillation are recorded by the photon detection system (PDS) modules, which is made of 60 optical modules of active area 207 × 8.6 cm each. 10 modules are inserted

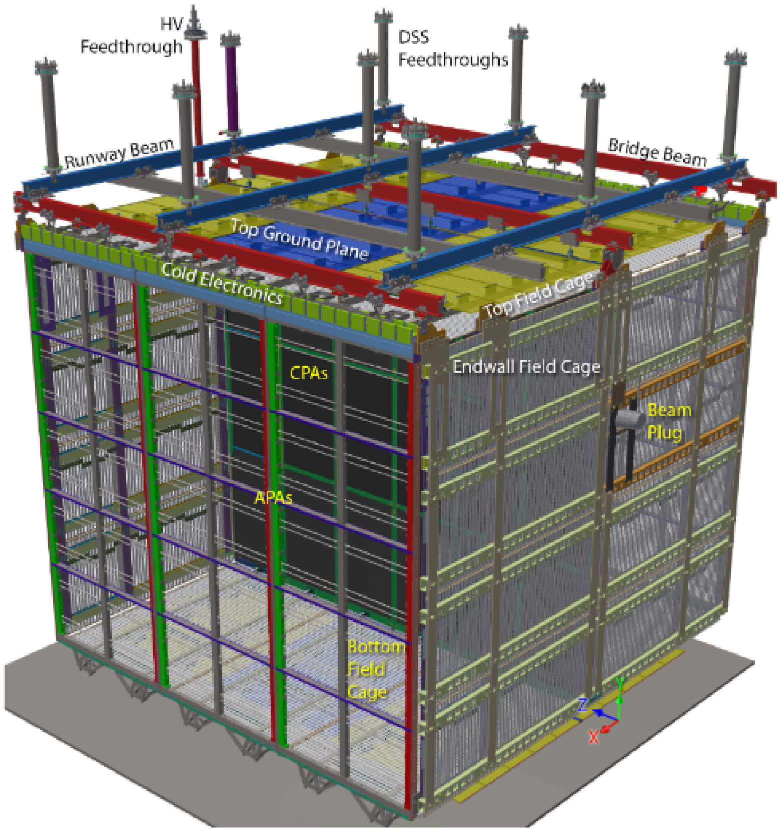

Figure 2: 3D model of the ProtoDUNE-SP detector with labelling of all major components.

into each APA frame, regularly spaced along the vertical direction. Each module combines a photon collector and a photon sensor. Three different collector designs were implemented in ProtoDUNE-SP: "double-shift light guides" [24], "dip-coated light guides" [25, 26], and ARAPUCA light traps [27]. Silicon Photomultiplier (SiPM) arrays from Hamamatsu and SensL vendors are deployed as sensors. The location of PDS modules in an APA frame and the three types of detector technologies are shown in Figure 3. The PDS performance is illustrated in detail in [14, 15].

3.2 Cosmic-Ray Tagger

The ProtoDUNE-SP detector is exposed to a flux of ~180 cosmic muons/(m^2 s). A fraction of these particles is tagged by a Cosmic-Ray Tagger (CRT, [14]): this is made of scintillator counters (strips) read by Silicon PhotoMultipliers, and it consists of four large assemblies, two mounted upstream and two downstream of the cryostat. Each assembly covers an area approximately 6.8 m high and 3.65 m wide. Modules are instrumented with 64 scintillator strips 5 cm wide and 365 cm long. Two-dimensional sensitivity is achieved by putting together groups of four modules into assemblies, with two modules being rotated by 90° with respect to the other two. It is then possible to reconstruct a muon track through the CRT, by drawing a line from hits in the upstream modules to hits in the downstream modules, the muon time-of-flight information dictating the width of the relative coincidence window. For the purposes of the ProtoDUNE detector studies, this allows

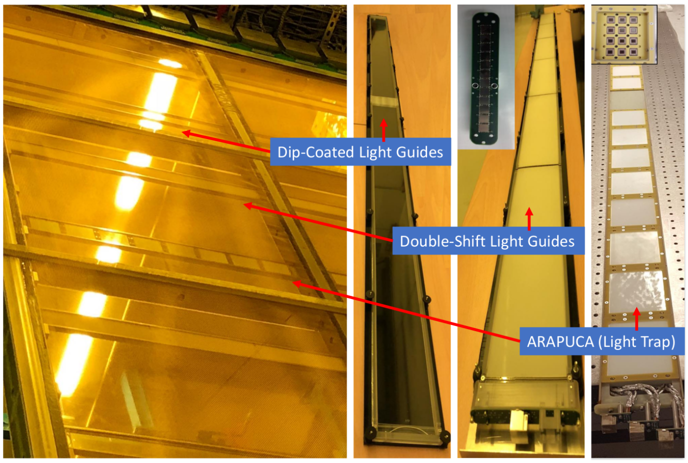

Figure 3: The three technologies of PDS modules shown inside the APA frame and on desk for comparison.

selecting uniform sets of cosmic-ray muons parallel to APAs, with a well defined direction and time stamp.

3.3 The X-ARAPUCA detectors in ProtoDUNE-SP

The ARAPUCA technology is based on light trapping, as discussed in [27]. In the base concept, trapping of 128 nm photons is achieved as follows: 128 nm photons hitting the detector are shifted down to 350 nm by a p-terphenyl (pTp) coating located on top of a dichroic filter, that features a 400 nm transparency cutoff. A second coating layer, with Tetraphenyl Butadiene (TPB), converts 350 nm photons to 420 nm. The upgrade of the technology (X-ARAPUCA) replaces the second coating layer with a WLS light guide, enhancing photon collection efficiency. [28]. In both versions, the obtained 420 nm photons are trapped inside the detector by the filter, fully reflective above the 400 nm cutoff, and they bounce back-and-forth until they reach the photosensors (cryogenic SiPMs).

Two ARAPUCA modules were installed in ProtoDUNE-SP for the first beam run, and they came out to be the preferred technology for the DUNE program, with a measured collection efficiency of 2% [15]. The upgraded X-ARAPUCAs will be deployed in the second beam run of ProtoDUNE-SP and later in DUNE FD1, however two prototypes were already inserted in ProtoDUNE-SP for the xenon doping run.

The two X-ARAPUCA (XA) detector units, called supercells, were installed on a dedicated support (see Figure 4). They are placed behind the APA-6, upstream with respect to the beam, at a distance of 22.7 cm from the frame (see Figure 5). The trigger for these detectors is not connected to the main ProtoDUNE DAQ. Instead, it is obtained from cosmic rays, through a standard triple coincidence of 15.5×44 cm plastic scintillators, located on the cryostat roof, 1.15 m far from the active volume. The three paddles select a solid angle of $\sim$0.43 steradians, resulting in an average trigger rate of about 1 Hz.

The two supercells are identical but for the presence, on the top one, of a fused silica window, which is opaque (awaiting numbers on transparency) to the 128 nm light and only transparent to photons from xenon. For this reason, this detector will be labeled in the following as “Xe-XA”.

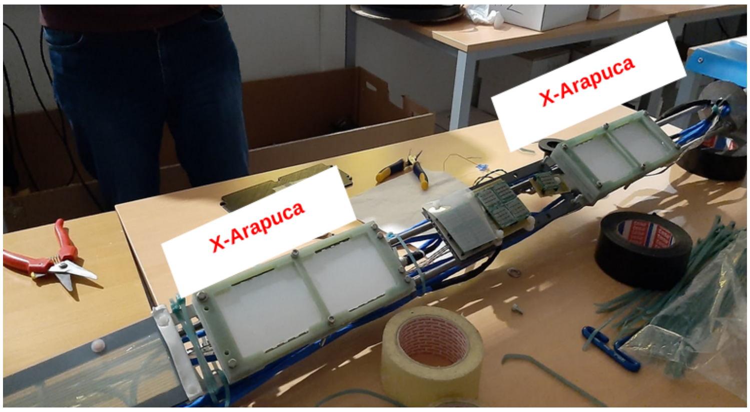

Figure 4: X-ARAPUCA detectors installed on a dedicated support (see 3D model in Fig. 5) and ready for insertion in the ProtoDUNE-SP cryostat.

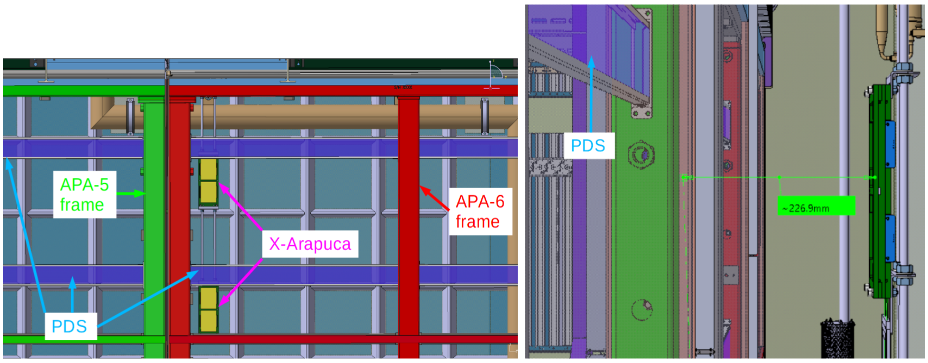

Figure 5: Top: front view of the two X-ARAPUCA detectors inside the ProtoDUNE-SP cryostat. In green, the frame of APA-5, in red the frame of APA-6, in blue the PDS bars. Bottom: side view, showing the position of the of the X-ARAPUCAs with respect to the APA frames and PDS.

The bottom supercell is instead sensitive to both argon and xenon light, and it will be referred to as "Ar+Xe-XA".

The X-ARAPUCA light collection efficiency was measured in two prototypes, one $10{\times}8$ cm^2 in size at Unicamp, Brazil [29] and the other 20×7.5 cm^2 in size at INFN Milano-Bicocca, Italy [30]: the latter is of the same type and size of those deployed in this work. From these tests, an average effective Photon Detection Efficiency (PDE) of ~2.3% is obtained.

Both X-ARAPUCA are equipped with Hamamatsu MPPCs S13360-6050VE [31] with a 6×6 mm^2 active area and 1.3 nF terminal capacitance. They were operated with a bias of 47.8 V (+4.8 V OV). This value was chosen to guarantee the SiPMs PDE >50% and to partially compensate for the lack of a cold front-end amplifier. Each supercell features two windows, both equipped with two arrays of four SiPMs positioned against the long sides of the WLS bar: the SiPMs within each array are readout in parallel, resulting in 4 readout channels per detector, and their signal is extracted via CAT6 cables. Readout is performed by a customized version of the standard SiPM Signal Processor (SSP) board in use for ProtoDUNE-SP run-1 [32].

4 Cryogenics operations for xenon doping in ProtoDUNE-SP

The ProtoDUNE-SP cryostat contains 770 tons of ultra pure LAr at 87.5 K, that is continuously purified through an ad-hoc cooling-recirculation plant. The Cryostat and the cryogenic plant are described in detail in [14].

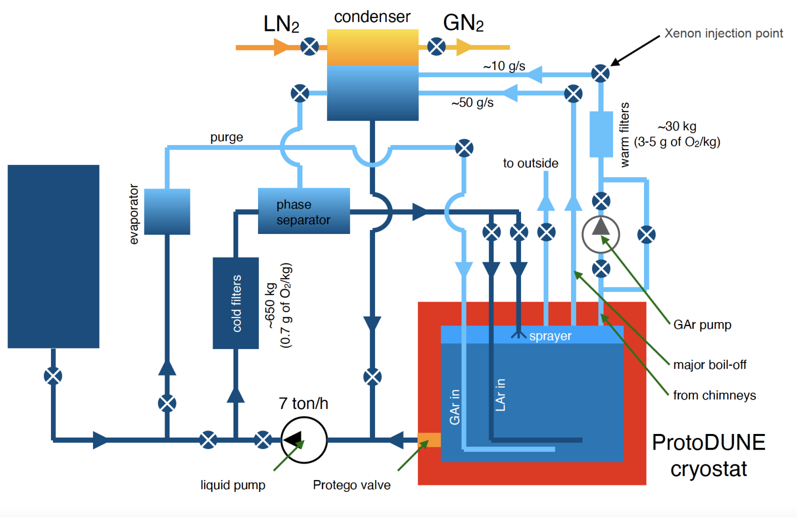

Figure 6: Schematics of ProtoDUNE-SP cryogenic system.

The system layout is depicted in Figure 6. It consists of two main circuits, for liquid and gas recirculation. The first circuit extracts LAr at the bottom of the cryostat by means of a cryogenic pump. The liquid is then forced through a cold purifier at a rate of $\sim$ 7 ton/hour. The purifier consist of a first section filled with molecular sieve optimized to remove polar molecules, such as H_2O or CO_2, and a second section containing copper deposited on alumina pellets, which adsorbs O_2 [33]. The purified liquid is injected back at the bottom of the cryostat at a slightly warmer temperature (and lower density) to allow its upward diffusion, thus ensuring a better mixing with the bulk LAr in the cryostat.

The gas circuit is meant to both stabilize the operating pressure in the cryostat, by re-condensing the boil-off gas continuously produced by the residual heat input, and to purify the gas argon present in the ullage and in the feed-through chimneys. Indeed, these areas are expected to be heavily polluted, due to the degassing of materials (mainly the cables) present in this area.

Preliminary tests performed by the collaboration at CERN, with smaller LAr-TPC prototypes equipped with gas recirculation/purification systems, demonstrated that xenon can be efficiently mixed with LAr by injecting it in the gas phase, before the re-condensation. Several mixing ratios were tested, showing that the Ar/Xe ratio must be above 10^3 to avoid the solidification of the xenon on the walls of the condenser. This *freeze-out* effect is observed as, at the highest xenon concentrations, the pipes of the condenser get clogged up and the argon re-circulation stops. For this reason, xenon injection in ProtoDUNE-SP was performed through the gas argon recirculation system (see Section 4.2).

4.1 Nitrogen contamination

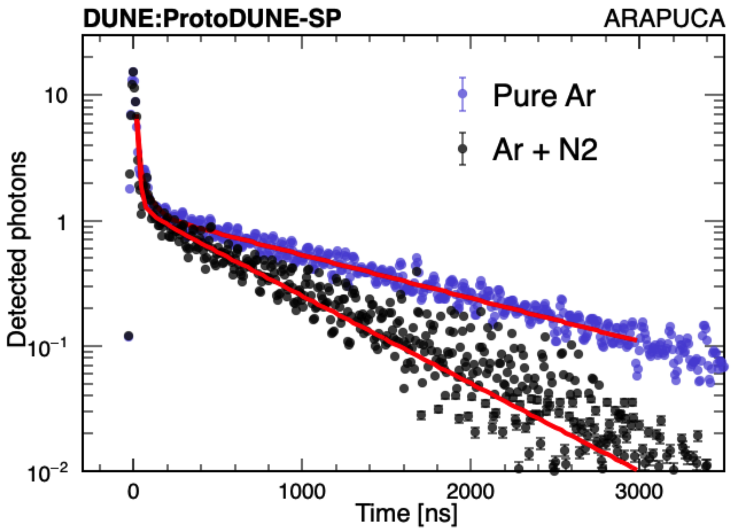

Figure 7: ProtoDUNE ARAPUCA module deconvoluted waveforms. Blue: "pure" Ar (before the air contamination), Black: after air contamination and purification (only N_2 contaminant is present). Pure argon waveform is scaled to have the same maximum amplitude on both waveforms.

As already mentioned, during the long cosmic run of ProtoDUNE-SP, a sudden failure in the warm gas re-circulation pump occurred, releasing a certain amount of air inside the detector. Molecules like O_2, CO_2 and H_2O were efficiently removed by the purification system, during the three weeks of recirculation through the filters, following the event. However, the system cannot remove N_2, which stayed in the detector until the end of the run. As mentioned in Section 2, nitrogen affects scintillation light emission, through the process of quenching. This effectively prevents the emission of scintillation photons from the slow component of the argon scintillation light.

As an example of the effect of N_2 quenching of LAr scintillation light, Figure 7 shows the typical profile of the scintillation light pulses for non-polluted LAr and LAr + N_2 after contamination, as obtained from ProtoDUNE SP data (specifically from the ARAPUCA module installed in APA 6).

By measuring the value of the decay-time constant of the argon triplet scintillation light component in both conditions [34], we can compute [23] the total amount of N_2 that is present in LAr: ~5.4±0.1 ppm, and derive the quantity leaked in during the accident: ~5.2±0.1 ppm. The initial (pre-accident) concentration estimated with this method is ~0.2 ppm N_2, compatible with the value provided by the LAr supplier (AirLiquide). This was regularly cross-checked with direct measurements performed during argon deliveries.

4.2 Xenon doping campaign of ProtoDUNE SP

The xenon doping run of ProtoDUNE-SP was started in February 2020 and lasted five months, with the goals of studying light emission in the presence of xenon, as well as long term stability and uniformity of the doped xenon inside the cryostat. It became even more important after the unexpected pollution event described above.

As mentioned, the xenon injection point is placed along the chimney boil-off re-circulation line (see Figure 6), after the gas purification filter but way before the condenser, to allow for full mixing within the gas flow. The maximum xenon mass flow rate was set to 36 g/h, to be well within the Ar/Xe ratio limit described above; this corresponds to 50 ppb/hour in the ProtoDUNE-SP detector. Based on the numerical (CFD) simulation of the LAr flow within the ProtoDUNE cryostat [35] [Asked to APB what to do with non-published references], the xenon injected at this rate is expected to be uniformly distributed in LAr within few hours. A detailed description of all steps of the doping procedure, and the lessons learned while performing it, is reported in Appendix A.

The run consisted in six injections, the last two of which were performed back-to-back over few days: for this reason, they are considered as one in the rest of the paper, from the point of view of the analysis. The amount of xenon injected in each step and the corresponding concentration inside the cryostat is summarized in Table 1. Combining all the doping steps, we injected 13.6 kg of xenon into the cryostat. This corresponds to 18.8 ppm of xenon concentration by mass in the 0.77 kt LAr of ProtoDUNE-SP.

Table 1: Six xenon doping steps in ProtoDUNE-SP. The dates, doped xenon mass in grams and concentration in ppm by mass are given for each doping step.

Doping	Date	Doped Xe[gr]	Doped Xe[ppm]
1	13-14 February 2020	776	1.1
2	26-28 February 2020	2234	3.1
3	3-8 April 2020	5335	7.4
4	27-30 April 2020	3192	4.5
5	15-16 May 2020	400	0.6
6	18-20 May 2020	1584	2.2

Extensive data taking during each injection and between the dopings was performed, both with the ProtoDUNE photon detection system and with the dedicated X-ARAPUCA. The evolution of the scintillation light emission was monitored during the whole campaign, as a function of the amount of injected xenon.

5 Analysis of the X-ARAPUCA data

Since the X-ARAPUCA data are collected with a standalone DAQ triggered by the three paddles outside the cryostat, we developed dedicated algorithms for data selection analysis. At the beginning of the run, an unexpected source of noise was found to be generated by the trigger electronics. In order to mitigate this noise, a subset of triggered events with no detectable physical signal was identified and their recorded pulses were averaged. The fraction of these empty events was approximately 7% of the total recorded triggers. We employed the averaged empty triggers to remove noise from the actual waveform and also correct an undershoot that was present in the signals.

X-ARAPUCA calibration is performed by extracting the Single Photo-Electron (SPE) shape for each channel of the two detectors. SPE pulses are usually searched for in the tail of each signal, i.e. well beyond the triggered pulse. Each integrated signal goes into constructing the SPE charge distributions, that are fitted with a double Gaussian function, modeling the pedestal and SPE peak. The averaged SPE waveform is then extracted by selecting the subset of pulses with charge within one sigma of the mean SPE value. Add definitions of SPE charge and pedestal.

This procedure was carried out regularly during the whole doping run, which allowed performing the first long-term stability test of the SiPMs installed in an X-ARAPUCA detector.

Fig. 8 shows the SPE charge stability along the entire run. The outcome of these quality tests demonstrated that the X-ARAPUCA system ran in stable conditions during the entire doping campaign.

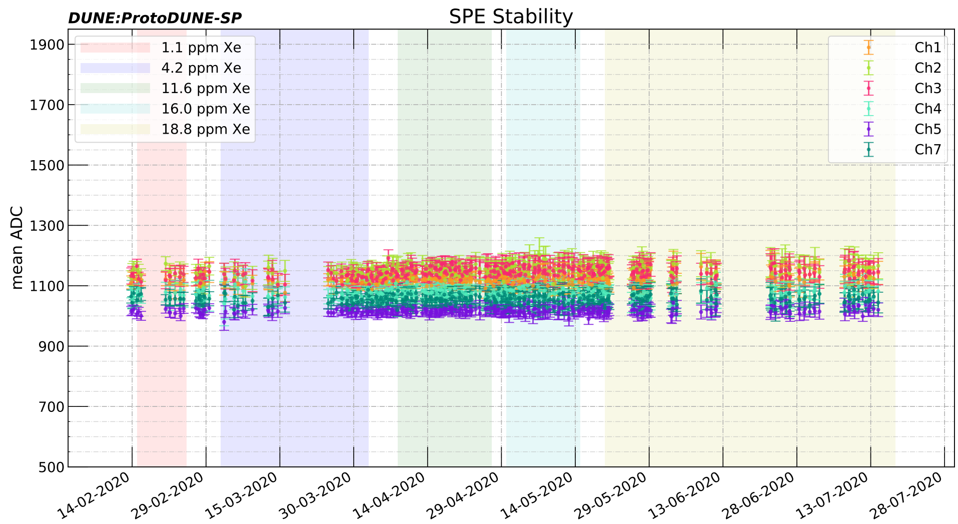

Figure 8: Mean SPE charge stability for all runs and each channel. Runs cover an overall six-month doping period, coloured areas represent specific dopings. To check whether the Y-axis represents charge (ADCC x ns) or peak amplitude (ADCc). Text refers to charge, whereas the Y-axis label to amplitude

5.1 Data selection and deconvolution

The data acquired with the X-ARAPUCA detectors were first converted into a ROOT TTree and pre-processed applying a moving average filter to reduce the white noise. For each waveform the integral, peak height in ADC counts and the peak time are computed and recorded.

The data are selected applying two main quality cuts, first the saturated events are discarded imposing a maximum on the peak-height parameter associated to each waveforms. The threshold value takes into consideration the electronics saturation level. Second we removed events with an ill-defined baseline or with a relevant pileup. These are events where a scintillation signal is present in the pretrigger region ($1 \div 200$ ticks) or in the ending of the signal ($1300 \div 2000$ ticks). The waveform are thus discarded if they cross a threshold of 10 photo-electrons in the respective defined regions.

The waveforms passing these cuts are averaged to reconstruct the response function of the detector. The information enclosed in these waveforms is the convolution of three main effects $S(t) = L(t) \otimes XA(t) \otimes h(t)$: the scintillation light time-profile $L(t)$, the X-ARAPUCA $XA(t)$ time-response and the electronics $h(t)$ response. The first is characterized by the light yield, the emission properties of the mixture (Ar+Xe+N_2) and by the light propagation including absorption and Rayleigh scattering. The second is characterized by the X-ARAPUCA response, in particular by the absorption and re-emission of the wavelenghtshifters. As the re-emission of TPB and PTP is considered below < 10 ns [CITATION], we can consider the time dependence of this effect negligible. The third effect is due to the transfer function of both sensors and the electronics. To retrieve the scintillation signal $L(t)$ containing the relevant physical information, this last effect needs to be deconvolved as the most relevant. In fact, the signal coming from SiPMs is proportional to the number of photons but has a time-extension of about 400 ns, comparable with scintillation signals.

To deconvolve this effect, a (time-dependent) template for the single photo-electron is needed. A filter for peak finding is implemented to search single photo-electrons in the pre-trigger region. Once selected, they are aligned at the same time and averaged; the resulting shape is then fitted. The fit function consists of a double exponential convoluted with a Gaussian to account for white noise: $h(t) = Gaus(t; \mu, \sigma) \otimes (\exp[-t/\tau_1] - \exp[-t/\tau_2])$. The two time constants represents respectively the SiPM avalanche discharge ($\tau_1 \sim 400$ ns) and the electronics shaping time.

More than one deconvolution technique was applied independently on the waveforms, to cross-check the results. One such technique is based on the Gold algorithm [36] and the parameters were optimized to minimize the reconstructed fast component of LAr, as well as the noise. Another technique makes use of a custom FIR filter to simultaneously de-noise the waveforms and filter out the shape of the single photo-electron response function. The filter employed is analogous to the one presented in [37], although it lacks the zero-area requirement. It is a finite-length cusp-like filter with a 33 ns flat top and the cusp shape parameter τ_s=33 ns. It is tailored for each of the 6 channels to properly take into account the individual exponential decay of channel response function.

5.2 Effects of xenon on LAr light

The effect of the energy transfer, as introduced in Section 2, is clearly exemplified in Figure 9. The plots show examples of waveforms that were deconvolved according to the technique introduced in the previous paragraph. The two panels refer to the two X-ARAPUCA detectors, showing superimposed waveforms at different concentrations of doping. The overall shortening of the pulse profile as a function of xenon concentration is evident in both cases. These data are collected with the presence of nitrogen, therefore the long tail of the typical argon signal is expected to be strongly reduced with respect to the non-polluted argon case (cfr. 7. In particular in the bottom panel of the figure, referring to the Xe-XA device, it is then possible to appreciate the concurrent effect of xenon: the increase in total light (the larger area under the pulse) is due to dimer excitation being transferred from argon to xenon.

After the SPE calibration, the absolute number of photons detected by the two X-ARAPUCA detectors can be extracted during the entire doping run. Fig. 10 shows that this number increases

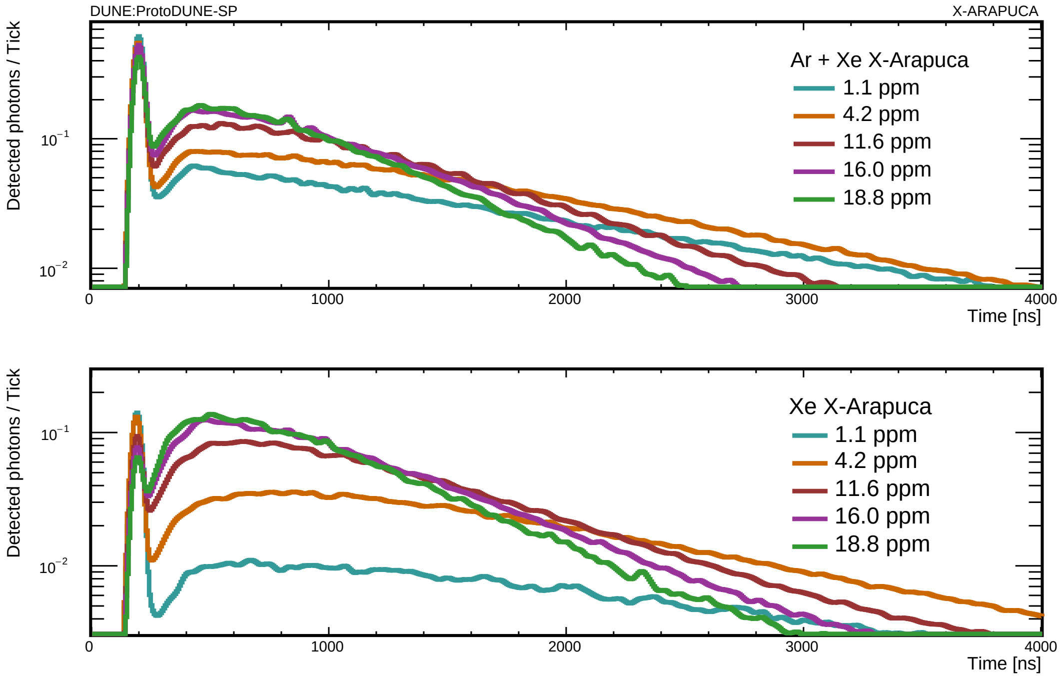

Figure 9: SPE-deconvolved average waveforms at different stages of xenon doping (after nitrogen pollution). Top panel: *Ar+Xe-XA*; bottom panel: *Xe-XA*. Only events with at least three detected photons in the Ar+Xe X-ARAPUCA module are selected.

during each injection and it remains stable during the monitoring periods, for both X-ARAPUCA. This general increasing trend testifies to the effectiveness of energy transfer, especially in the presence of N_2. Indeed, the light that was lost after the pollution event appears to be recovered once xenon starts competing with N_2-induced quenching. We note that, while it is widely reported in literature citation that xenon effects on light emission extend up to few hundreds ppm concentration, in these conditions and with these detectors, the increase appears to flatten out at the level of around 16 ppm of xenon, indicating a possible saturation effect. It worth noting though that further data collected in the following two months are compatible with a flat trend, which hints to a stability in time of the xenon doping effect.

In this picture it is possible to appreciate the effect of the presence of the TPC electric field on light production, as well. Since the absolute amount of light produced is considered here, drops in the number of photons is expected when the electric field is on. Indeed, its presence drifts away electrons that would otherwise recombine with their parent ions, thus reducing the overall light output of the detector. The mentioned dips are clearly visible on the data-sets of both X-ARAPUCA.

The actual amount of liquid argon scintillation light (128 nm) that is shifted to xenon light (178 nm) is the observable chosen to evaluate in a more quantitative way the efficiency of the energy transfer between argon and xenon excimers. This is defined as the ratio between the xenon light and the total light detected for each run, that is, in this case, the ratio of the average light seen by

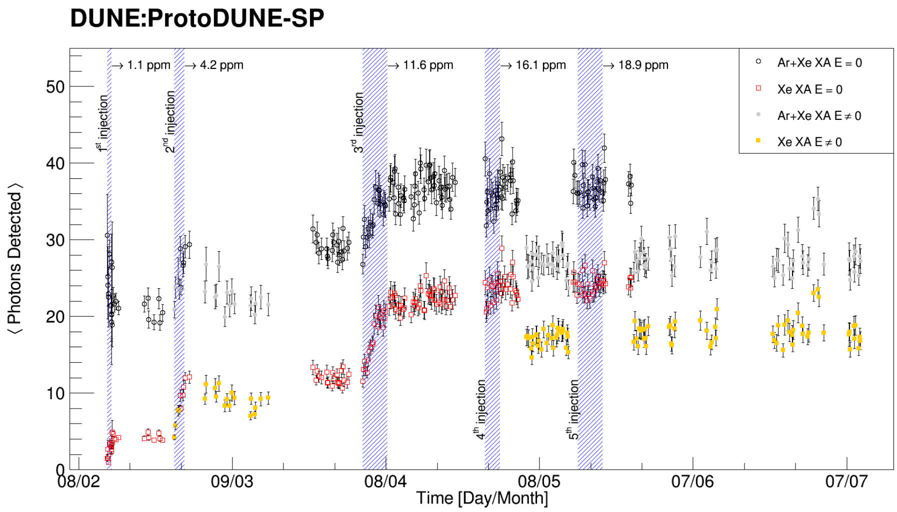

Figure 10: Light collected by the two X-ARAPUCA modules, in units of detected photons. The amount of collected light increases at each doping. Sudden drops are caused by the activation of the HV system of ProtoDUNE-SP and, hence, the presence of the electric field. Shaded areas show the time when xenon was injected.

the Xe X-ARAPUCA (only sensitive to xenon, see Sec. 3.3) to the average light seen by the Ar+Xe X-ARAPUCA (sensitive to the total light).

$$\text{Fraction} = \frac{\text{Xe light}}{\text{Ar light} + \text{Xe light}} \equiv \frac{\langle \gamma_{\text{Xe XA}} \rangle}{\langle \gamma_{\text{Ar+Xe XA}} \rangle} \tag{5.1}$$

Figure 11 shows the above ratio as a function of time, increasing at each doping. Also in this case, the trend tends to flatten out at around 16.1 ppm, reaching a stable value of 0.65. In this configuration, one can assume that the triplet component of the argon light is completely drained by the presence of xenon. The ratio remains stable outside the injection periods (dashed regions).

It is worth noting that in this case, since only relative amounts of light are considered, the trends of the two data-sets with and without the TPC electric field are superimposed. This suggests no detectable interference between the electric field presence and the argon-xenon energy transfer process, at least at the level of this local measurement. Some differences appear to arise only when considering the profile of collected light as a function of the distance of the track from the light sensors (see Section 6).

Further information about the effect of xenon presence can be extracted by surveying the evolution of the amount of so-called "fast" and "slow" light components independently, as a function of time.

Figure 12 shows what is here defined as "slow light", i.e. the superposition of the residual triplet argon scintillation light and part of the xenon-converted light. This is defined from the integral of the waveform in a fixed time-window, starting 11 time-ticks (∼74 ns) after the trigger until the end of the recorded pulse. how was this value chosen? The number of photons from this light component is shown to increase with xenon concentration, with a trend quite similar to

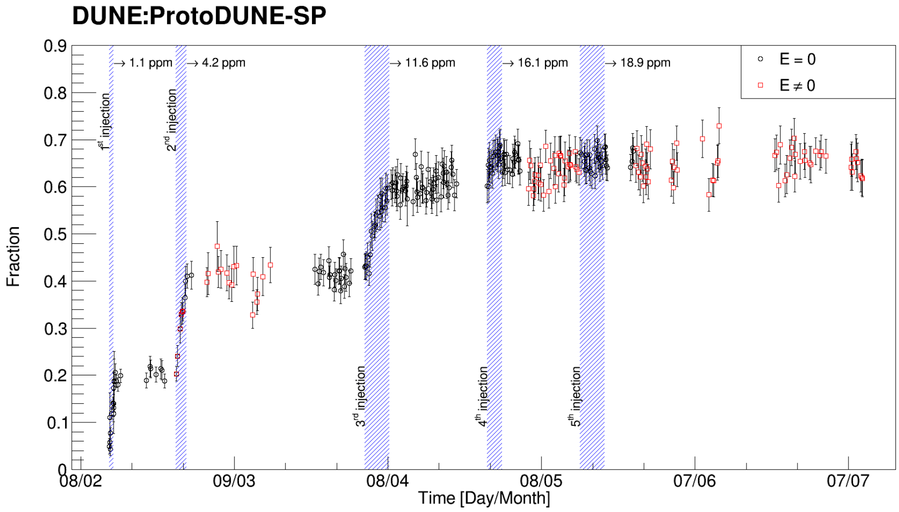

Figure 11: Fraction of the argon light (128 nm) that is converted to xenon light (178 nm): $\frac{\mathrm{Xe}}{\mathrm{Ar+Xe}}$. The ratio increases with the doping and reaches a plateau around 0.65 for xenon concentration greater than 16.1 ppm. The red points correspond to data collected with the nominal TPC electric field, while black points refer to data with no electric field. Shaded areas indicate xenon injections.

that of the overall light output produced in Figure 10. This is expected and consistent with the fact that the energy transfer process involves the argon long-lived triplet state (see Section 2. As a further evidence of the origin of this light increase, the trends observed for the two X-ARAPUCA are almost identical, i.e. it can be traced back entirely to 178 nm xenon scintillation light.

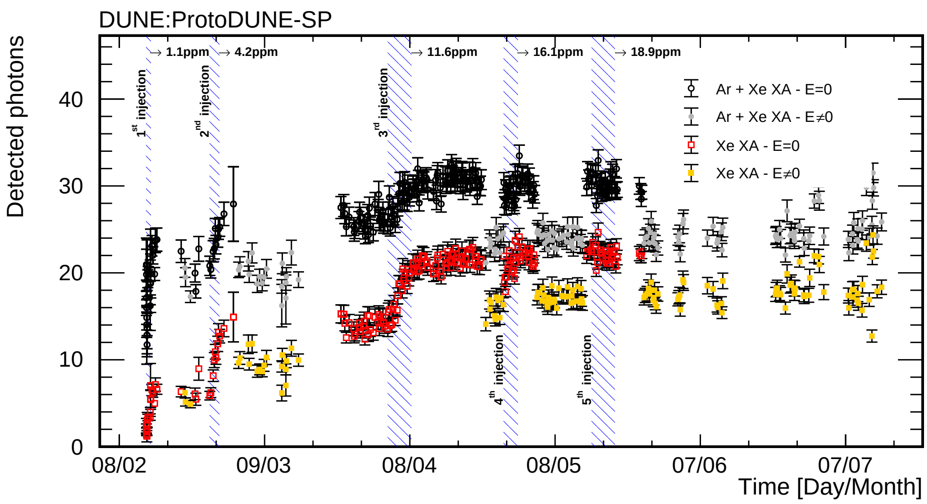

Figure 12: Time survey of the mean number of photons in the slow light component detected by the *Ar+Xe-XA* and by the *Xe-XA*, for runs with (E≠0) and without (E=0) electric field. Shaded areas indicate xenon injections. Only events with at least three detected photons in the Ar+Xe X-ARAPUCA module are selected.

Figure 13 shows the evolution of the “fast” light component with time. This is defined as the fraction of the integral of the waveform taken between the trigger time and 10 time-ticks after that Same comment as above on 10/11 ticks. The plot shows a very quick drop of this light component during the first doping period, followed by a pretty reduced and stable output throughout the rest of the run.

The quick drop of the fast light that is observed at the beginning of the doping comes as unexpected. Indeed, it cannot be explained *a priori* by the xenon energy transfer process, as the argon singlet decay time (τ_s = 6 ns) is much shorter that the time required for the Ar_2^* - Xe interaction to take place. However, there are studies in literature ([38]) that report an actual absorption of the argon light by xenon: according to these results, the absorption profile of xenon partially overlaps with the 128 nm scintillation peak of argon, which has a FWHM of around 10 nm. The absorption process seems to be saturating already at the lowest concentrations of xenon, which is consistent with what is observed in our data. Going back to Figure 9, one can notice that also in this case such draining effect of the fast component is more clearly visible in the xenon-only sensitive X-ARAPUCA (bottom panel).

Figure 13 and figure 9 show that despite the process described above, on average one-/two-*fast*, i.e. within 70 ns, photons are detected by the Xe-XA for Xe doping ≥ 1.1 ppm: they might be due to Cherenkov emission from cosmic rays secondary particles crossing the device entrance window, wavelength-shifted light escaping other PDS modules and entering the not light-tight device inner volume, and spurious events inside the latter. Questions to exclude this is noise: these ’one/two photons" are those recorded in time with fast component in the other detector. Which window of coincidence is chosen? the 74 ns of the ’fast light’ integral or an interval around the trigger time from the other x-arapuca?

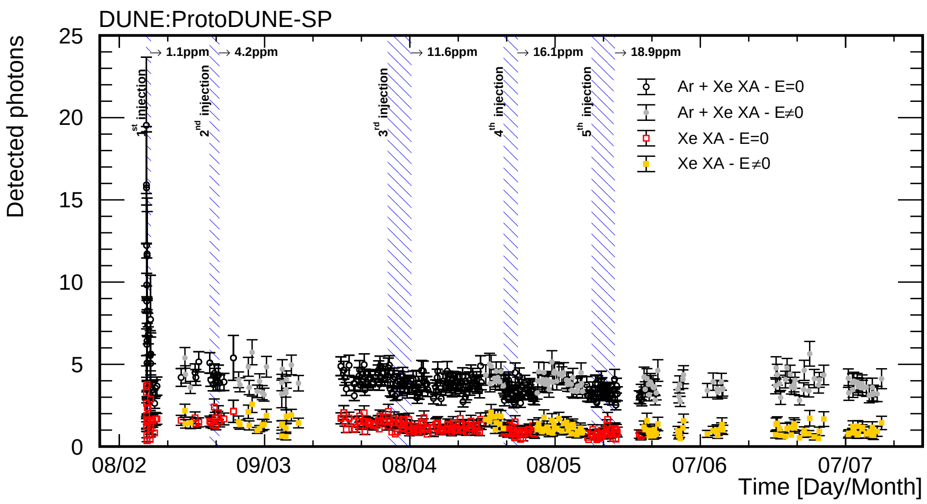

Figure 13: Time survey of the mean number of photons in the fast light component detected by the *Ar+Xe-XA* and by the *Xe-XA*, for runs with (E≠0) and without (E=0) electric field. Shaded areas indicate xenon injections. Only events with at least three detected photons in the Ar+Xe X-ARAPUCA module are selected.

The analysis of the X-ARAPUCA data implies a local measurement of the xenon effect on argon scintillation light, made on a specific set of data: vertical and almost vertical cosmic muons. As a whole, the analysis yields a general confirmation of the assumed model of argon-xenon energy transfer, as known from literature. It also confirms the successful implementation of the doping in ProtoDUNE-SP and hints at a reasonable stability in time: the effect of xenon increases during injections and appears not to degrade soon after the doping is completed. These data do however leave some open questions, especially concerning the fast light component detected by the X-ARAPUCAs. This will be addressed in a second publication, exploiting with further analysis and comparing these data with similar sets collected with the other DUNE prototype present at CERN, ProtoDUNE Dual Phase (DP).

6 Analysis of the ProtoDUNE-SP PDS

The Photon Detection System of ProtoDUNE-SP provides an independent handle to observe the changes in the scintillation medium as a consequence of doping or contamination. It also has the added benefit of allowing direct comparison with the original run period before nitrogen contamination [15]. To this end, the data-set discussed in this Section is divided into multiple epochs: a period before xenon doping and nitrogen contamination, described as the first ProtoDUNE-SP run; a period after the first run, with only nitrogen present in the drift volume; and a xenon doping period, where xenon was injected over a period of few months. All periods feature different configurations of the TPC electric field, which varies from zero to the nominal setting (500 V/cm) significantly changing the total absolute amount of light available. All of the following ProtoDUNE PDS studies use light collected from through-going cosmic-ray muons selected in coincidence with the CRT.

6.1 Triggering, data selection, and collected light

Triggering in ProtoDUNE-SP relies on the central DAQ and typically involves a coordination between two or more subsystems. For the ProtoDUNE-SP PDS, two major triggering schemes exist which both depend on a coincidence between the upstream and downstream modules of the Cosmic-Ray Tagger (CRT). The trigger coincidence window length, pre-scaling, and trigger mask have varied throughout the run configurations as indicated by the red lines in each of the Figures from 14 to 17. If the TPC is available and at the proper potential, a CRT coincidence is coordinated with through-going tracks, allowing a comparison of the orientation of the track, reconstructed by the TPC, to the vector which intersects the center of both triggered CRT modules strips. A quality cut is made on single tracks that meet the TPC reconstruction and selection criteria, have a viable trigger, and pass a quality cut of $\cos\theta > .999$, indicating a deviation of less than a degree between track from TPC and trigger from CRT. If the TPC is not available, a selection is made based on matching distinct PDS coincidences across APAs requiring at least two photon detectors in two different APAs within a time coincidence of 13 μs.

The light collected from the selected sample is summed across a single detector and assigned a *radial distance*, which is defined as the straight line distance from the photon detector to the track when they are in the same XY-plane. A Gaussian or Poissonian fit to the collected light at each cm of radial distance is performed to obtain the most probable value, which represents the expected amount of light observed from a passing muon at a given radial distance where the choice of distribution depends on the bin statistics. An analysis of the average collected light as a function of time and with different trigger periods is shown for different regions of the detector and distinct SiPMs in Figures 14 to 17. Despite the variations in triggers, the average amount of light collected does not change appreciably with trigger variation. All figures draw a consistent picture across the detector volume, SiPM models and detection technologies, when compared with the X-ARAPUCA results produced in the previous Section. The average amount of light detected in ProtoDUNE drops after the nitrogen contamination and then it increases again in steps, with each new doping with xenon. Data collected with and without the TPC electric field consistently show two parallel trends of increase, due to the different available total amount of scintillation light. The data from runs with the TPC electric field on show larger spread, as anticipated, due to a wide number of trigger configurations used for these runs.

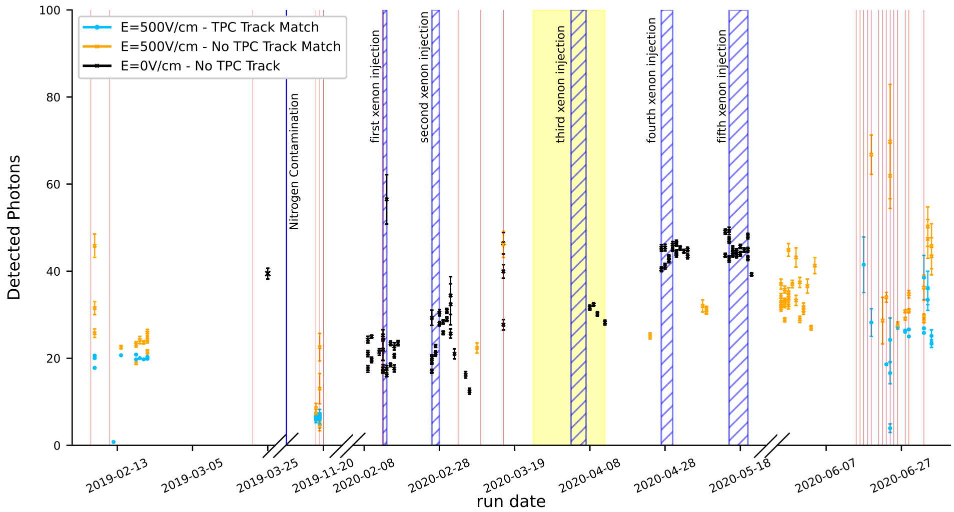

Figure 14: The figure shows the average number of photons detected in the ARAPUCA on beam left in the PDS over the entire nitrogen contamination and xenon doping period. Red lines indicate changes in the trigger configurations; blue lines indicate changes in the scintillation medium through nitrogen contamination or xenon injection, the yellow band indicates a period of operation where only APA 3 and APA 6 were operational.

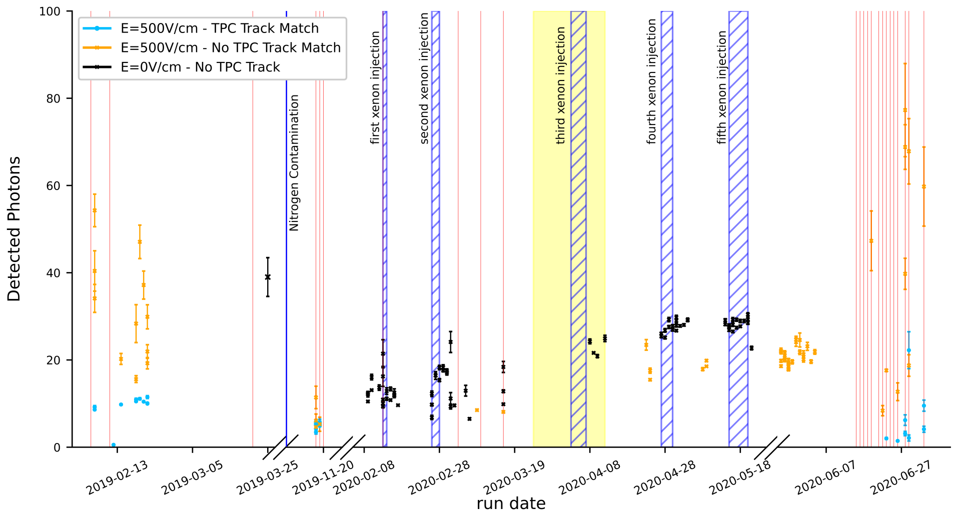

Figure 15: The figure shows the average number of photons detected in the ARAPUCA on beam right in the PDS over the entire nitrogen contamination and xenon doping period. Red lines indicate changes in the trigger configurations; blue lines indicate changes in the scintillation medium through nitrogen contamination or xenon injection, the yellow band indicates a period of operation where only APA 3 and APA 6 were operational.

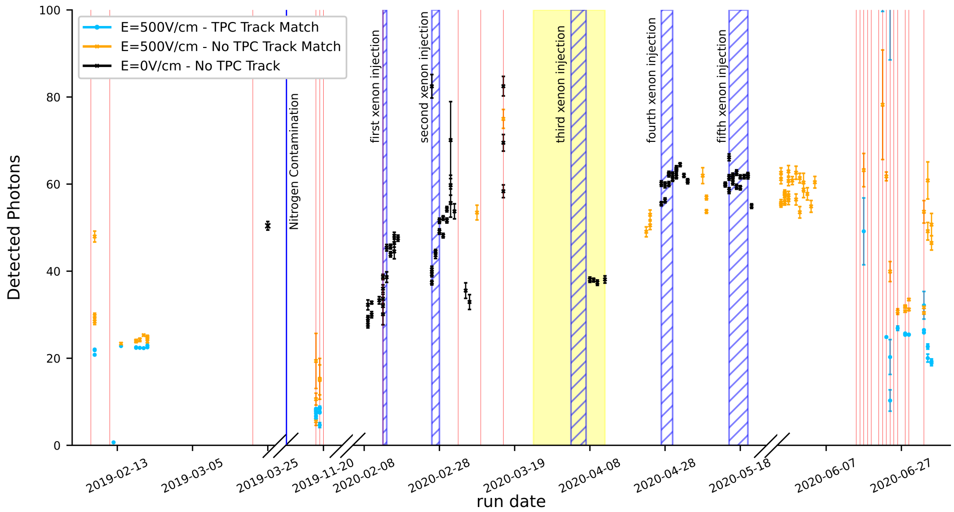

Figure 16: The figure shows the average number of photons detected in the Double shifted light guides with Hamamatsu MPPC sensors throughout the entire PDS over the entire nitrogen contamination and xenon doping period. Red lines indicate changes in the trigger configurations; blue lines indicate changes in the scintillation medium through nitrogen contamination or xenon injection, the yellow band indicates a period of operation where only APA 3 and APA 6 were operational.

6.2 Light recovery due to xenon injection

As described in the previous Section, the amount of collected light by the ProtoDUNE PDS and the changes in the characteristic light-pulse profiles (waveforms) can supply critical information about how the injected xenon significantly alters the character of the scintillation light produced in the detector. Furthermore, the use of the ProtoDUNE-SP PDS also allows constructing attenuation curves that track the amount of detected photons as a function of the previously defined *radial distance* between the tracks and the photon detectors. The following plots refer mainly to data collected by the non-beam side ARAPUCA, i.e. those in the Left TPC, or *Beam-Left*, BL, with respect to the beam direction (see Section 1). The phrase *Pure LAr* in the plots legends is short for the data relative to the period before the nitrogen contamination. Fig. 18 clearly indicates that the amount of light collected by the non-beam side ARAPUCA drops after the nitrogen contamination, but then increases again significantly after the xenon injection. The plots of the right column also highlight that the light recovery, quantified by the ratio of the light after doping over the amount of light before nitrogen contamination, increases with the distance from the photon detectors. Once again, comparing plots (a) to (d) with plots (e,f) the described behaviour is completely independent of the presence of the TPC electric drift field. This result is confirmed and enforced when comparing it with the same plots coming from data collected with other photon detection technologies: as an example, Figure 19 reports the same attenuation curves and ratios of light collected, with respect to the period before nitrogen contamination, for the non-beam side double shifted light guides, equipped with both SensL and Hamamatsu SiPMs. Figures 18 (b,f) and 19 (bottom panels) confirm

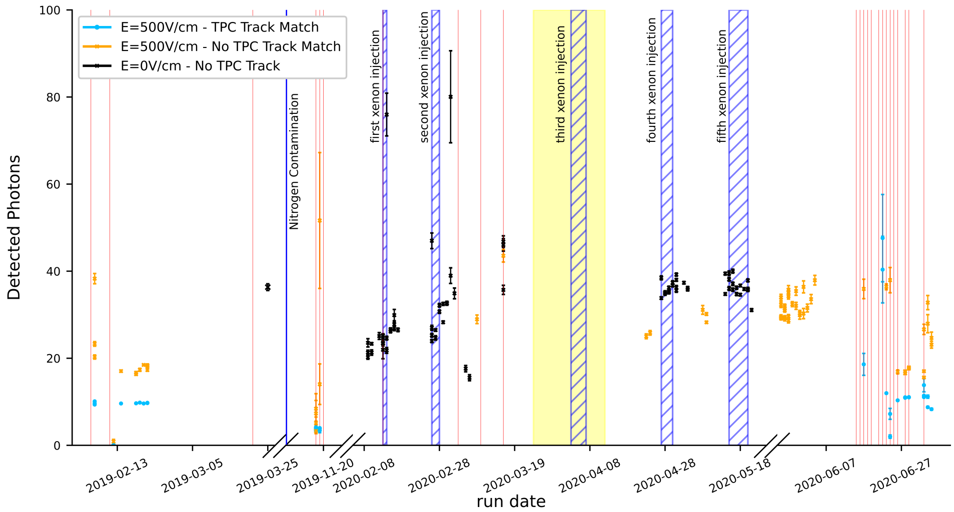

Figure 17: The figure shows the average number of photons detected in the Double shifted light guides with SensL SiPM sensors throughout the entire PDS over the entire nitrogen contamination and xenon doping period. Red lines indicate changes in the trigger configurations; blue lines indicate changes in the scintillation medium through nitrogen contamination or xenon injection, the yellow band indicates a period of operation where only APA 3 and APA 6 were operational.

that, due to the larger Rayleigh scattering length in LAr at 178 nm, with respect to that at 128 nm, the uniformity of response as a function of the distance from the detection plane increases after the doping. This mitigates the intrinsic non-uniformity of the DUNE PDS, which is installed only in the proximity of the TPC anode, i.e. inside the APAs.

The details of the overall light increase with respect to the nitrogen contamination period shown in the comparison of the characteristic light waveforms across the doping period: Figure 20. Events used in these plots are a subgroup of all events showed in Fig. 18 (c) and (d). Selection was made using tracks with a defined geometry. The selected events mean radial distance is $\sim$ 250 cm, with standard deviation of $\sim$ 30 cm. The selection is needed as, given the differences between the argon and xenon light propagation, the waveform shape and integrals are expected to change with the distance of the event from the detector; see Figure 18.

Comments by Flavio: not explained where factor 5 below and 95% values come from; no discussion on how this compares with expectation and present models/measurements. BR: response, values come directly dividing average light from before and after doping and before and after contamination. I don't know if we have expectation because we haven't done doping with so much nitrogen contamination. This is a 'new' mixture and I'm not sure we understand microphysics of absorption and energy transfer between molecules. Panels (a,b) demonstrate that, as the concentration of xenon increases, the slow[2] component of the characteristic argon waveform is increased by at least a factor of five. On the other hand, the characteristic argon fast component

[2]For the analysis of the PDS data, the same definitions of *slow* and *fast* component of the scintillation light, in terms of interval of integration and given in Section 5, still hold.

is significantly reduced right after the first doping, but then it remains very stable throughout the following doping steps. These trends are consistent with what is obtained from the analysis of the X-ARAPUCA data, but on a global detector scale and with a different sample of tracks. Panels (c,d,e) in Figure 20 summarise the changes in the average number of detected photons across the full xenon doping period for the slow and fast components of the scintillation light, as well as for the total collected light.

Comment by Flavio on fig 18 and related text. three results in these plots, to be better discussed / separated: attenuation with and without Xe; light loss due to nitrogen (not shown for x-arapuca, so 'new'); effect of rayleigh, with higher coll. eff. at large distance / lower at short distance.

To reinforce the statement made at the end of the previous subsection, the presented analysis confirms on a global, detector-wide level, the results obtained on a local level with the dedicated X-ARAPUCA detectors in Section 5. The comparison of results from different areas of the main active volume and the studies of the collected light profile as a function of distance from the photon detectors hint strongly at a successful doping procedure, which led to uniformly distributing xenon across the detector volume. Such an encouraging result represents the necessary stepping stone towards the implementation of xenon doping at the much larger scale of the DUNE far detectors.

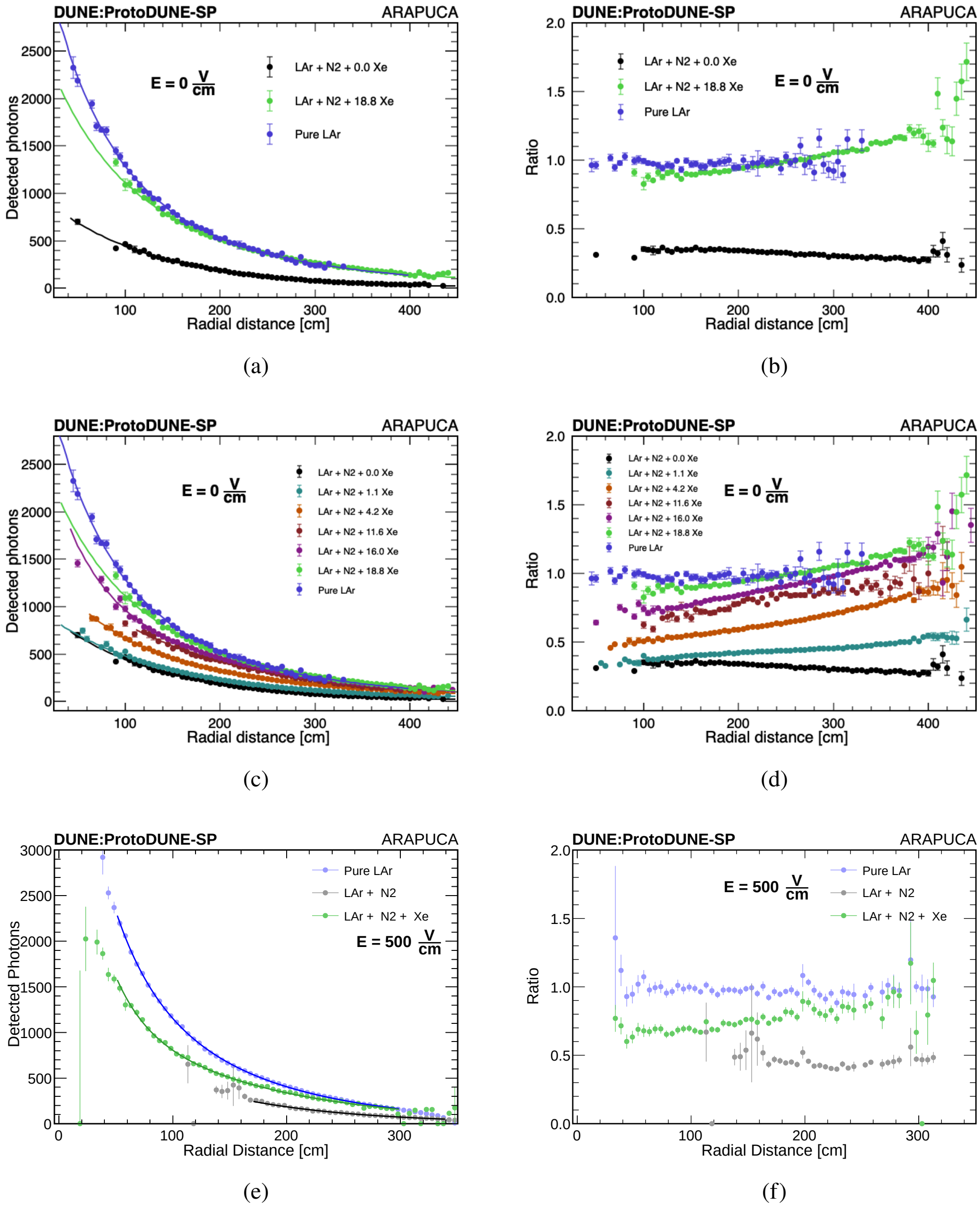

Figure 18: Light recovery demonstrated through attenuation curves after xenon injection with the non-beam side PDS ARAPUCA. The left column of plots shows the collected light versus radial distance, while the right column shows the ratio of collected light relative to the pure LAr and nitrogen-contamination periods. The top and bottom rows of plots show the measurement made without and with TPC electric field, respectively. The middle plots detail the gradual increase of collected light with increasing xenon concentration, with no drift field.

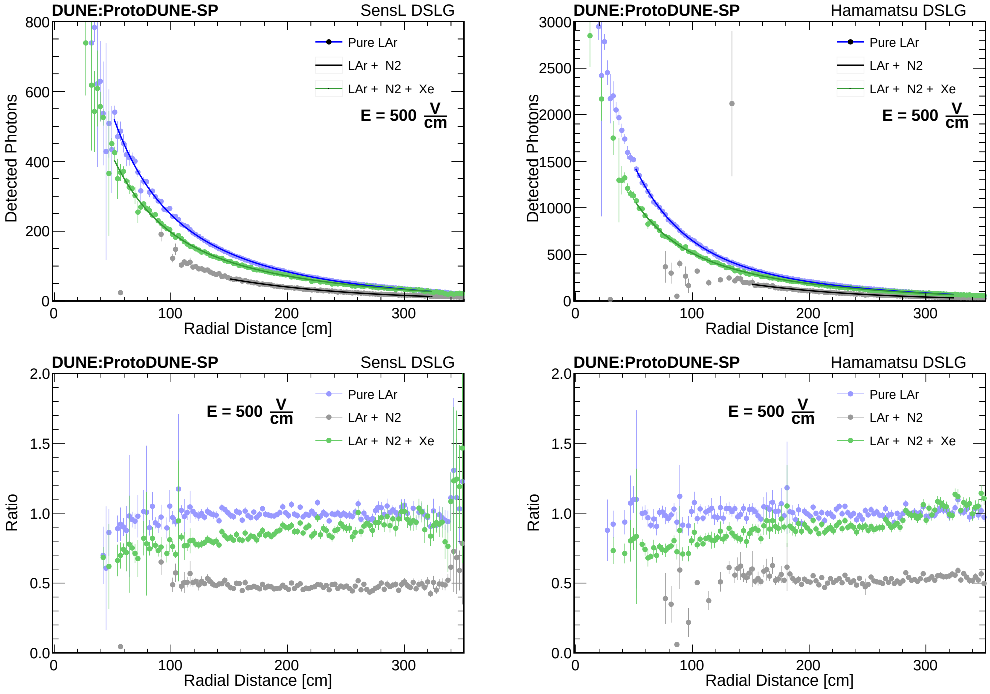

Figure 19: Light recovery as demonstrated through attenuation curves for the non-beam side double shifted light guides, divided by sensor technology, with the TPC drift field on. The top plots represent the collected light versus radial distance, whereas the bottom plots represent the ratio of collected light relative to the pure LAr and nitrogen-contamination periods.

7 Charge reconstruction in liquid argon doped with xenon

During the xenon doping run, the operation of the ProtoDUNE SP TPC was monitored in order to understand whether the presence of the dopant would affect the charge collection.

A useful monitor of the stability of the ProtoDUNE TPC performance is the so-called *TPC signal strength*. In ProtoDUNE-SP, the primary contribution to charge deposits in the LAr is ionization from cosmic rays. The amount of collected charge is evaluated for each collection wire by summing all the calibrated charge deposits, over those regions where the signal is significantly above the noise level for the channel. The fraction of the originally produced ionization charge actually reaching each collection wire depends on the purity of the LAr, on the voltages applied to the wires and cathode planes, as well as on space charge effects [15]. The calibrated response of the detector relies on the electronics modules gain, which was evaluated with test-charge injections and was stable over the course of the run [39].

Figure 21 shows the TPC signal strength before, during and after the xenon filling, for those periods where APA data were collected with voltages at or near nominal values. Each point is evaluated by averaging the calibrated charge over all good collection wires in an APA for few thousand randomly triggered events, with acquisition windows of 3 ms in each event. The figure includes a line at 93 ke/channel/ms, typical reference for nominal voltages and high purity. The drop in signal strength on all APAs are due to episodes where the purity dropped.

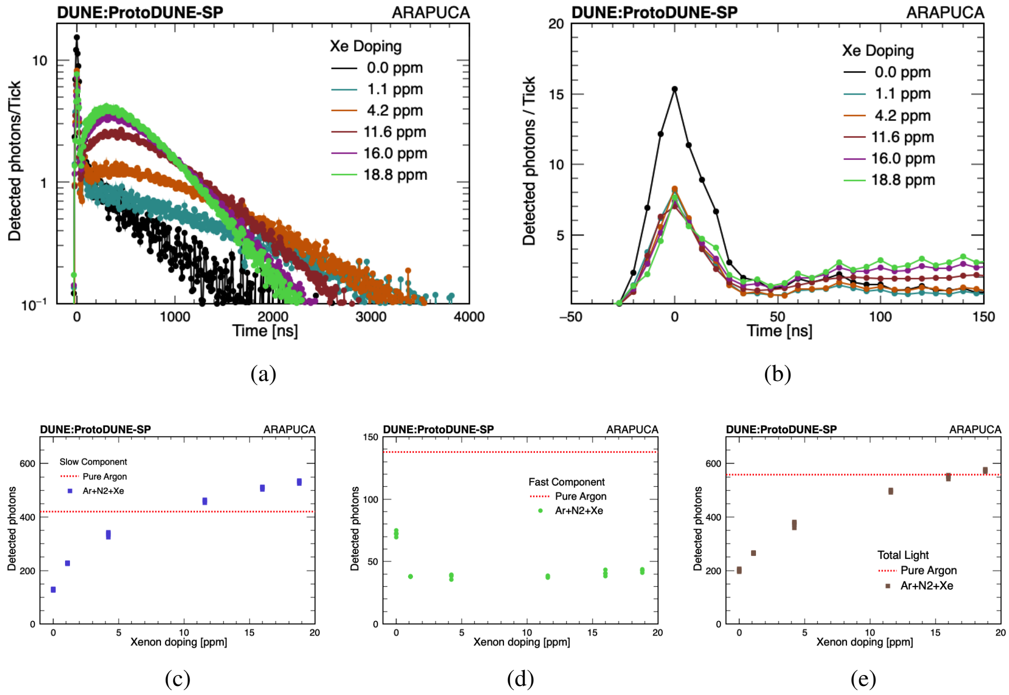

Figure 20: Top row: non-Beam Side ARAPUCA deconvoluted waveforms, changing in shape with the concentration of xenon. Bottom row: evolution of the fast, slow light component and total light as a function of xenon concentration, in the nitrogen contaminated scintillation medium (details of track selection for these plots is reported in text).

The xenon doping period is highlighted in light yellow, whereas the darker yellow refers to maximal xenon concentration. One can see that the average TPC signal strength in standard conditions remains at its nominal value before, during and after the xenon doping. This indicates that xenon has no observable effect on the fraction of charge reaching the collection wires, and therefore that it can be safely used in the DUNE far detectors.

8 Conclusions - NOT CORRECTED YET

In this paper we presented the design, commissioning and analysis of the xenon doping run of ProtoDUNE-SP. This run was performed in 2020 and represents the first demonstration that a large size (770 tons) LArTPC can be safely operated with xenon at the level of $\sim$ 20 ppm. The performance of the detector was validated using both the built-in PDS and a dedicated X-ARAPUCA detector triggered in standalone mode and expressly installed before the run. Both systems provide consistent results: the 128 $\longrightarrow$ 178 nm light shift is effective already at xenon concentrations of a few ppm and it reaches a plateau at $\sim$ 16 ppm. Its effects are to shorten the PDS time response and enhance its uniformity in space. It also helps recovering about 95% of the light originally lost due to nitrogen pollution, because of an air leak developed in a gas recirculation pump.

The collected data show that already at 10 ppm concentration most of the light that was lost due to the N_2 pollution of LAr is recovered, thanks to the shift of the excited states from Ar_2^* to Xe_2^*.

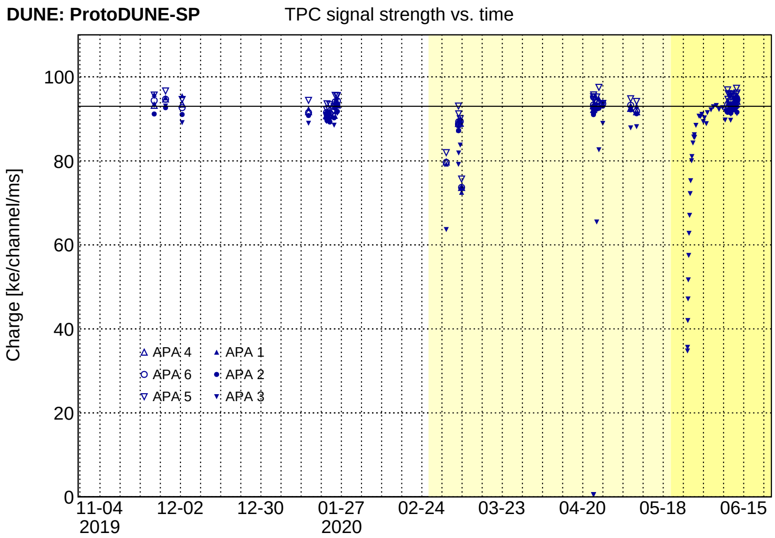

Figure 21: Signal strength versus time, near the time when xenon was injected. The doping period is highlighted in light yellow, whereas darker yellow represents xenon at maximum concentration. The drop at the beginning of the light yellow area corresponds to a drop in purity following the first injection (see Appendix A). Data points for APA 3 are consistently lower than other APAs after turning on the electric field, and steadily recover in the first few days, due to a problem on its grid plane biasing.

In particular, the Ar_2^* triplet state is mostly affected by the pollution and the doping, being relatively long-lived. More detailed insights confirm that, due to the longer Rayleigh scattering length of the xenon light, the profile of the collected light versus the distance of the interaction from the detection plane is more uniform after the doping. These results are independent of the presence of the TPC electric drift field. The analysis of the ionization charge collected by the anode planes during and after the doping demonstrates that xenon up to 18.8 ppm does not affect the performance of the TPC.

The operation of doping with xenon a LArTPC at the ~kt scale was a never attempted feat, and resulted in a smooth and successful run. The data collected during this campaign corroborate the original DUNE Collaboration idea of using xenon to enhance the Photon Detection System of a LArTPC like DUNE, and of reducing the intrinsic non-uniformity of the PDS, which is installed only in the APA. Furthermore, use of xenon can mitigate the effect of unexpected LAr contaminations during the foreseen 10-20 year-long DUNE data taking period. These results will be extremely valuable to understand this operation mode for the DUNE far detector modules and other massive LArTPCs.

A Details on xenon injections in ProtoDUNE SP and contaminations

Here, a more in depth description of the actual xenon injection procedure in ProtoDUNE-SP is reported. As mentioned in Section 4.2, the xenon injection point is placed along the chimney boil-off re-circulation line, way before the argon condenser, in order to ensure full argon-xenon mixing within the gas flow.

In order to precisely control the amount of gas introduced at any step of the doping, xenon bottles were placed on a scale connected to the detector slow control system. A dedicated purification filter (SAES Micro-Torr) was installed on the line, followed by a mass flow-meter, calibrated for xenon, and a pressure gauge. The entire line installed between the xenon bottle and the connection with the argon re-circulation system was kept under vacuum by a separate pumping system. Xenon pressure, flow and bottle weight were continuously recorded by the slow control system. Figure 22 illustrates the xenon injection set up.

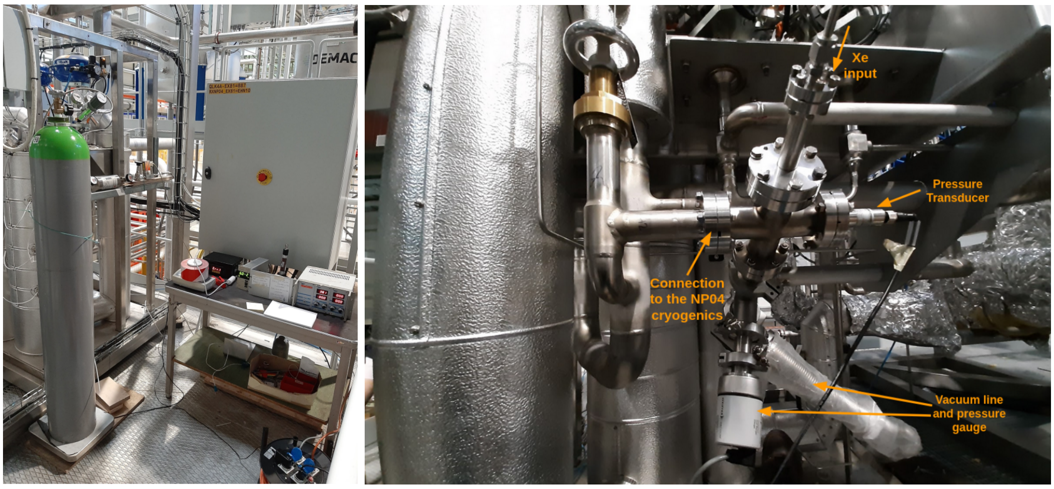

Figure 22: Left: the xenon bottle on the scale connected to the gas purifier, the mass flow-meter and the injection line. Right: the UHV injection line equipped with vacuum/pressure monitoring devices and connected to the NP04 gas circulation system.

The doping was performed with three different bottles of xenon. The first one (containing about 3 kg of gas) was rated with a purity grade 5.0[3], without any specifications on upper limits on fluorinated compounds. However, during the first injection, a sizable degradation of the free electron lifetime was recorded within the LArTPC, as shown in Figure 23.

As a consequence, xenon injection was stopped and a set of spectrographic/ chromatograpic analyses were performed at CERN [40] (Same comment as for CFD simulations: is this public?). Electro-negative impurities were identified as C_2F_6 ($\sim$ 10 ppm Comment by Flavio: is this 10 ppm confirmed? This should correspond to the total amount of contaminants in a 5.0 grade bottle.) plus traces of SF_6 and CO_2. These compounds, that can be present in xenon at the ppm level as residuals of the distillation process, are known to be highly electro-negative (several orders of magnitude higher that Oxygen [41]), hence they can significantly degrade the free electron lifetime in LAr

[3]The purity grade refers to the fractional amount of gas in ther bottle. 5.0 corresponds to 99.999% of xenon in the bottle.

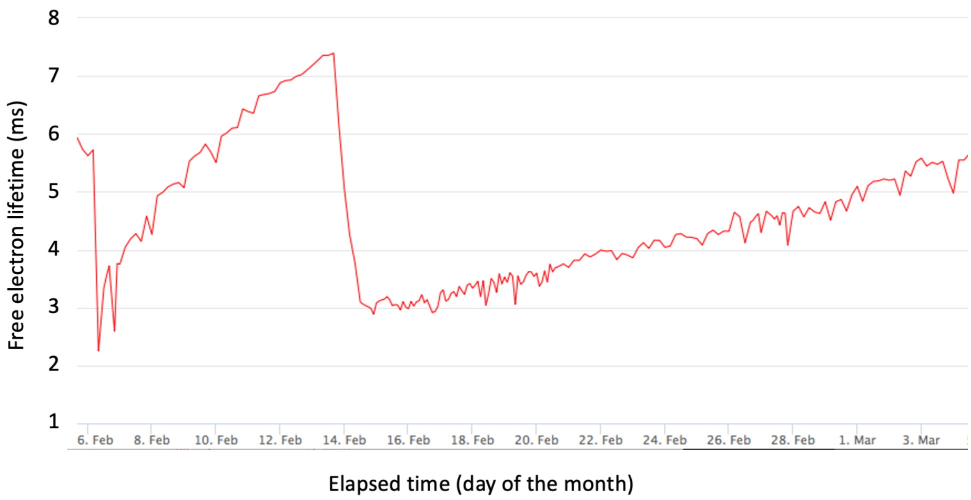

Figure 23: Left: Free electron lifetime measurement in ProtoDUNE-SP performed with dedicated purity monitors. The linear drop recorded around February 13th, coincides with the first xenon injection and is attributed to the presence of fluorinated contaminants in the bottle. The subsequent recovery rate, due to LAr recirculation, is about a factor 8 to 10 slower than in previous recoveries (exemplified in the increase shown prior to the injection). This suggests that the ProtoDUNE purifiers can absorb fluorinated compounds, though with a factor ~10 lower efficiency, with respect to oxygen.

even at concentrations of few ppt. After this episode, free electron lifetime in ProtoDUNE SP slowly recovered with a time constant of ~30 days, indicating that the purifiers are able to absorb fluorinated compounds, albeit with an efficiency about 10 times lower than that for oxygen.

Two additional xenon bottles (containing about 17.5 kg each) were then acquired, rated with a purity grade of 5.5 and a specified SF_6 content certified by the producer to be lower than 20 ppb (following standard procedures set by CERN for the ATLAS and ALICE experiments). No sizable electron lifetime degradation was observed during the subsequent injections with this higher purity xenon.

References

[1] C. Rubbia, "The liquid-argon time projection chamber: a new concept for neutrino detectors", Technical Report CERN-EP-INT-77-8, CERN, Geneva, 1977.

[2] S. Amerio et al., "Design, construction and tests of the ICARUS T600 detector", *Nuclear Instruments and Methods in Physics Research Section A: Accelerators, Spectrometers, Detectors and Associated Equipment* **527** (2004), no. 3, 329–410, doi:https://doi.org/10.1016/j.nima.2004.02.044.

[3] R. Acciarri et al., "Design and construction of the MicroBooNE detector", *Journal of Instrumentation* **12** (feb, 2017) P02017–P02017, doi:10.1088/1748-0221/12/02/p02017.

[4] C. Anderson et al., "The ArgoNeuT detector in the NuMI low-energy beam line at fermilab", *Journal of Instrumentation* **7** (oct, 2012) P10019–P10019, doi:10.1088/1748-0221/7/10/p10019.

[5] C. E. Aalseth et al., “Darkside-20k: A 20 tonne two-phase LAr TPC for direct dark matter detection at LNGS”, *The European Physical Journal Plus* **133** (2018), no. 3, 131, doi:10.1140/epjp/i2018-11973-4.

[6] B. Abi et al., “Volume I. introduction to DUNE”, *Journal of Instrumentation* **15** (aug, 2020) T08008–T08008, doi:10.1088/1748-0221/15/08/t08008.

[7] B. Abi et al., “Volume IV. the DUNE far detector single-phase technology”, *Journal of Instrumentation* **15** (aug, 2020) T08010–T08010, doi:10.1088/1748-0221/15/08/t08010.

[8] B. Abi et al., “Supernova neutrino burst detection with the deep underground neutrino experiment”, *The European Physical Journal C* **81** (2021), no. 5, 423, doi:10.1140/epjc/s10052-021-09166-w.

[9] S. Kubota, M. Hishida, M. Suzuki, and J. Ruan(Gen), “Liquid and solid argon, krypton and xenon scintillators”, *Nuclear Instruments and Methods in Physics Research* **196** (1982) 101–105.

[10] M. Suzuki, M. Hishida, J. Ruan(Gen), and S. Kubota, “Light output and collected charge in xenon-doped liquid argon.”, *Nuclear Instruments and Methods in Physics Research* **A327** (1993) 67–70.

[11] M. Hofmann et al., “Ion-beam excitation of liquid argon.”, *The European Physics Journal* **C73** (oct, 2013) 2618, doi:10.1140/epjc/s10052-013-2618-0.

[12] C. Wahl et al., “Pulse-shape discrimination and energy resolution of a liquid-argon scintillator with xenon doping.”, *Journal of Instrumentation* **9** (2014) P06013, doi:10.1088/1748-0221/9/06/P06013.

[13] D. Akimov et al., “Fast component re-emission in xe-doped liquid argon.”, *Journal of Instrumentation* **14** (sep, 2019) P09022, doi:10.1088/1748-0221/14/09/P09022.

[14] D. Collaboration et al., “Design, construction and operation of the protodune-sp liquid argon tpc”, arXiv:2108.01902.

[15] B. Abi et al., “First results on ProtoDUNE-SP liquid argon time projection chamber performance from a beam test at the CERN neutrino platform”, *Journal of Instrumentation* **15** (dec, 2020) P12004–P12004, doi:10.1088/1748-0221/15/12/p12004.

[16] Aprile, E. et al., “The xenon1t dark matter experiment”, *Eur. Phys. J. C* **77** (2017), no. 12, 881, doi:10.1140/epjc/s10052-017-5326-3.

[17] D. Akerib et al., “The large underground xenon (lux) experiment”, *Nuclear Instruments and Methods in Physics Research Section A: Accelerators, Spectrometers, Detectors and Associated Equipment* **704** (2013) 111–126, doi:https://doi.org/10.1016/j.nima.2012.11.135.

[18] T. Doke and K. Masuda, “Present status of liquid rare gas scintillation detectors and their new application to gamma-ray calorimeters”, *Nuclear Instruments and Methods in Physics Research Section A: Accelerators, Spectrometers, Detectors and Associated Equipment* **420** (1999), no. 1, 62–80, doi:https://doi.org/10.1016/S0168-9002(98)00933-4.

[19] M. Babicz et al., “A measurement of the group velocity of scintillation light in liquid argon”, doi:10.1088/1748-0221/15/09/p09009.

[20] K. Majumdar and K. Mavrokoridis, “Review of liquid argon detector technologies in the neutrino sector”, *Applied Sciences* **11** (2021), no. 6, doi:10.3390/app11062455.

[21] A. Neumeier et al., “Intense vacuum ultraviolet and infrared scintillation of liquid ar-xe mixtures”, *EPL (Europhysics Letters)* **109** (jan, 2015) 12001, doi:10.1209/0295-5075/109/12001.

[22] A. Buzulutskov, "Photon emission and atomic collision processes in two-phase argon doped with xenon and nitrogen.", *Europhysics Letters* **17** (mar, 2017) 39002, doi:10.1209/0295-5075/117/39002.

[23] R. Acciarri et al., "Effects of nitrogen contamination in liquid argon", *Journal of Instrumentation* **5** (jun, 2010) P06003–P06003, doi:10.1088/1748-0221/5/06/p06003.

[24] B. Howard et al., "A Novel Use of Light Guides and Wavelength Shifting Plates for the Detection of Scintillation Photons in Large Liquid Argon Detectors", *Nucl. Instrum. Meth.* **907** (2018) 9–21, doi:10.1016/j.nima.2018.06.050, arXiv:1710.11233.

[25] L. Bugel et al., "Demonstration of a Lightguide Detector for Liquid Argon TPCs", arXiv:1101.3013.

[26] Z. Moss et al., "A Factor of Four Increase in Attenuation Length of Dipped Lightguides for Liquid Argon TPCs Through Improved Coating", arXiv:1604.03103.

[27] A. Machado and E. Segreto, "ARAPUCA a new device for liquid argon scintillation light detection", *Journal of Instrumentation* **11** (feb, 2016) C02004–C02004, doi:10.1088/1748-0221/11/02/c02004.

[28] A. Machado et al., "The X-ARAPUCA: an improvement of the ARAPUCA device", *Journal of Instrumentation* **13** (apr, 2018) C04026–C04026, doi:10.1088/1748-0221/13/04/c04026.

[29] E. Segreto et al., "First liquid argon test of the X-ARAPUCA", *Journal of Instrumentation* **15** (may, 2020) C05045–C05045, doi:10.1088/1748-0221/15/05/c05045.

[30] C. Brizzolari et al., "Enhancement of the x-arapuca photon detection device for the DUNE experiment", doi:10.1088/1748-0221/16/09/p09027.

[31] Hamamatsu, "MPCC S13360-2050VE/3050VE/6050VE", https://www.hamamatsu.com/eu/en/product/type/S13360-6050VE/index.html.

[32] DUNE Collaboration, "The Single-Phase ProtoDUNE Technical Design Report. ", Technical Report FERMILAB-DESIGN-2017-02, Jun, 2017. 165 pages.

[33] A. Curioni et al., "A regenerable filter for liquid argon purification", *Nuclear Instruments and Methods in Physics Research Section A: Accelerators, Spectrometers, Detectors and Associated Equipment* **605** (2009), no. 3, 306–311, doi:https://doi.org/10.1016/j.nima.2009.04.020.

[34] T. Heindl et al., "Table-top setup for investigating the scintillation properties of liquid argon", *Journal of Instrumentation* **6** (feb, 2011) P02011–P02011, doi:10.1088/1748-0221/6/02/p02011.

[35] E. Voirin, "ProtoDUNE LAr Flow Simulation- Impurity field and Charge Density.", Technical Report DUNE DocDB Doc # 928, Jun, 2019.

[36] M. Morháč et al., "Background elimination methods for multidimensional coincidence γ-ray spectra", *Nuclear Instruments and Methods in Physics Research Section A: Accelerators, Spectrometers, Detectors and Associated Equipment* **401** (1997), no. 1, 113–132, doi:https://doi.org/10.1016/S0168-9002(97)01023-1.

[37] GERDA Collaboration, "Improvement of the energy resolution via an optimized digital signal processing in gerda phase i", *The European Physical Journal C* **75** (Jun, 2015) 255, doi:10.1140/epjc/s10052-015-3409-6.

[38] A. Neumeier et al., "Attenuation of vacuum ultraviolet light in pure and xenon-doped liquid argon —an approach to an assignment of the near-infrared emission from the mixture", *EPL (Europhysics Letters)* **111** (jul, 2015) 12001, doi:10.1209/0295-5075/111/12001.

[39] D. Adams et al., “The ProtoDUNE-SP LArTPC electronics production, commissioning, and performance”, *Journal of Instrumentation* **15** (jun, 2020) P06017–P06017, doi:10.1088/1748-0221/15/06/p06017.

[40] M. Corbetta, R. Guida, and B. Mandelli, “Gas chromatograph and mass spectrometer analysis of Xenon bottles used by the ProtoDUNE Experiment.”, Technical Report CERN EP-DT-FS, Mar, 2020.

[41] G. Bakale, U. Sowada, and W. F. Schmidt, “Effect of an electric field on electron attachment to sulfur hexafluoride, nitrous oxide, and molecular oxygen in liquid argon and xenon.”, *The Journal of Physical Chemistry* **80** (nov, 1976) 2556–2559, doi:10.1021/j100564a006.